

## **Detection and monitoring of super sand storm and its impacts on Arabian Sea- Remote sensing approach**

**Pravin D. Kunte\* and Aswini M.A.**

National Institute of Oceanography, Council of Scientific & Industrial Research, Dona Paula, Goa - 403 004, India.

### **Abstract**

The present study addresses an intense sand storm event over the Persian Gulf and its transport over the Arabian Sea region and the Indian sub-continent using satellite observations and measurements. MODIS data are used to analyze the temporal variation of the dust events that occurred from 17 to 24 March 2012 with the strongest intensity on 20 March over Arabian Sea. MODIS images are examined to provide an independent assessment of dust presence and plume location and its migration over Arabian Sea to Indian sub-continent. Dust enhancement and dust detection procedure is attempted to demarcate a dust event. Dust source, transportation path and dissipation is studied using source-back-tracking, wind speed & direction and remote sensing methods. Two possible hypothesis describing source and transportation path are discussed. This study concludes that super dust storm is a result of combination of two hypothesis. Further an attempt is made to investigate impact of super dust storm on Arabian Sea by studying sea surface temperature and chlorophyll *a* variability during the events. It is noted that sea surface temperature is decreased and chlorophyll *a* concentration increased during the post event period. The present study demonstrates usage of remote sensing data and geospatial techniques in detecting and mapping of dust events and monitoring dust transport along specific regional transport pathways over land and ocean.

Keywords Sand storm . MODIS data . Storm monitoring . Remote sensing .

Air pollution . Arabian Sea

---

\* Author to whom correspondence should be addressed.

Dr. Pravin D. Kunte

National Institute of Oceanography, Council of Scientific & Industrial Research, Dona Paula, Goa - 403 004, India; e-mail: [dr\\_pdkunte@yahoo.com](mailto:dr_pdkunte@yahoo.com)

Aswini M.A.

National Institute of Oceanography, Council of Scientific & Industrial Research, Dona Paula, Goa - 403 004, India

## 1. Introduction

Large quantities of dust with particle size less than 10 microns are dispersed in earth's atmosphere by wind-driven processes. This dust is of significant scientific interest owing to its ability to potentially alter climate, reduce local visibility, cause health problems in humans, and affect biogeochemical cycles in the world's oceans (Redmond et al., 2010). The erosion, transport and deposition of this kind of particle matter create hazards when it affects human activities (Bocconel, 2010). Locally, dust storms result in a low visibility, creating dangers for road and air transport. There is also an environmental concern because of the severe dust erosion occurring, and also because has an impact on the nutrient budget of oceanic ecosystems by providing a source of Fe to fertilize ocean regions that would otherwise be nutrient starved (Liss and Turner, 2000).

Despite the increased anthropogenic emissions due to the population growth, the air quality in south Asia is also affected by mineral particles from dust storms and smoke from naturally occurring biomass burning (Ichoku et al., 2004). Deserts in western Asia produce large amounts of mineral dust particles that enter in the atmosphere. Dust is considered to be one of the major sources of tropospheric aerosol loading, and constitutes an important key parameter in climate aerosol-forcing studies (Kaufman et al., 2002; Tegen 2003; Huang et al., 2006; Slingo et al., 2006). Therefore, the real-time monitoring of dust storms is essential for sustainable development, and for climate change and environmental research in the world. Satellite-based measurements for monitoring these atmospheric constituents are a viable proposition since ground-based measurements are limited in space and time (Liu et al., 2008; Papadimas et al., 2008).

It is well known that dust mineral particles influence the earth's radiation balance and the climatology mainly in two ways: first by reflecting and absorbing incoming and outgoing radiation and secondly by acting as cloud condensation nuclei. Dust aerosols strongly affect visibility, perturb the radiation balance in the Earth–Atmosphere system, and also cause serious biological and ecological effects (Boccone1, 2010). The significant dust effects on global climate, meteorology and atmospheric dynamics, ecosystems and human health are highlighted in detail in review studies (Goudie and Middleton 2001; Engelstaedter et al., 2006; Choobari et al., 2014).

Desert wind can transport dust to thousands of kilometers away from the source regions. Particle sizes are initially determined by their source regions. Therefore, due to the high spatial variability of the dust plume characteristics along its transport, remote sensing is an established method for the detection and mapping of dust events (Kaskaoutis et al., 2008; Badarinath et al., 2010) and has recently been used to identify the dust-source locations with a varying degree of

success (Washington et al., 2003; Alpert et al., 2004; Vachon et al., 2004; Bullard et al., 2008; Baddock et al., 2009). To this respect, the passage of dust over land and ocean and the variation along its transport have been monitored by satellite sensors with resolutions varying from high (hundreds of meters) to low (hundreds of kilometers); among others AVHRR (Yingjie Li et al., 2013), METEOSAT (Banks et al., 2013), MODIS (Baddock et al., 2009), TOMS AI (Goa and Washington, 2009), MSG-SEVIRI (Schepanski et al., 2007), and SeaWIFS (Antoine and Nobileau 2006). However, the ability to use remotely-sensed data both to detect a dust plume and identify the location from where it has originated is affected by several factors including the radioactive transfer properties of the material emitted, the radioactive properties of the ground/ocean surface over which the plume is transported, the size and density of the dust plume, the time of satellite overpass relative to dust emission, the presence or absence of cloud, the horizontal and vertical plume trajectory, and the sensor characteristics and radioactive transfer model used to detect dust (Baddock MC, et al., 2009).

For high temporal and spatial resolution, satellite remote sensing could be an ideal method for studying the process of dust storms as they begin, develop, and fade away at large scales. Compared to other remotely sensed data, MODIS has advantages as more useful narrow channels and high spatial and radiation resolution. MODIS visible/near infrared (VNIR) and thermal infrared (TIR) bands are helpful for cloud screening. Moreover, because MODIS are on EOS-AM1 Terra and EOS-PM1 Aqua satellites, MODIS can provide more real-time data (daytime and nighttime) to study dust storm motion processes.

Sand storm event which occurred during the 2<sup>nd</sup> half of March 2012 period reduced the visibility drastically and Meteorologist termed it as “Super Sand Storm” (Fig. 1). The storm while passing over Arabian Sea, might have dropped large amount of dust particles in the Sea, which might have affected the marine ecosystem.

### *1.1. Objective*

The main objectives of this study are 1) to detect the storm and monitor migration of this super sand storm using multi-sensor measurements and geospatial techniques, 2) to validate the existence and migration path of the super sand storm with CALIPSO and back trajectory study, 3) to analyze the impact of this sand storm event on the variability of chlorophyll\_a concentration and sea surface temperature of the Arabian Sea, and 4) to study the possible relation between the SST, chlorophyll and dust storm loading.

## 2. Materials

The Moderate-resolution Imaging Spectroradiometer (MODIS) is a payload launched into Earth orbit by NASA in 1999 on-board the Terra (EOS AM) Satellite, and in 2002 on-board the Aqua (EOS PM) satellite. The instruments capture data in 36 spectral bands ranging in wavelength from 0.4  $\mu\text{m}$  to 14.4  $\mu\text{m}$  and at varying spatial resolutions (2 bands at 250 m, 5 bands at 500 m and 29 bands at 1 km). Desert dust can be detected via satellite observations in the ultraviolet (0.315–0.4 $\mu\text{m}$ ) via absorption, visible (0.38–0.79 $\mu\text{m}$ ) via scattering and thermal infrared via contrasting land/aerosol emissivity (Baddock et al., 2009). Each MODIS sensor passes the same site twice a day: one in the daytime orbit for all thirty-six bands and the other in the nighttime orbit only for the thermal bands 20-25 and 27-36. Totally, four measurements are collected every day with two MODIS sensors. The data used in this study are of version 5 L1B measurements issued by NASA. Each MODIS file (referred to as a “granule”) collects consecutive measurements within five minutes, typically 203 scans, covering an area with 2030 km (along-track) by 2330 km (cross-track) (Nishihama et al., 2000; Isaacman et al., 2003). Cloud-Aerosol Lidar and Infrared Pathfinder Satellite Observations (CALIPSO) satellite is part of the "A Train", flying in formation with several other satellites (Aqua, Aura and CloudSat). CALIPSO data is used to study vertical column of dust storm. Other sensors on MODIS also provide information on sea surface temperature (SST) and chlorophyll *a* to study primary productivity.

## 3. Methods

Over the recent decades, several methodologies have been used to assess deflation, transport, and deposition of the dust: 1) Reconstruction of air-mass trajectories is calculated to trace dust deposits back to their source area. 2) Analysis of the concentration and composition of certain tracers in the dust itself, and comparing them to soils and sediments from possible source areas. This method has the advantage of being useable for palaeo-atmospheric circulation and palaeo-dust transport studies, whereas satellite imagery study and air-mass back trajectories are restricted to relatively recent times. 3) Regional or global atmospheric circulation models, mapping of dust deposition and analyses of source fingerprints.

In general, the dust detection algorithms use 7 of the 36 available MODIS channels to exploit the spatial and spectral contrast features of the dust (Guo and Liang, 2006). Listed in terms of channel index; central wavelength; native spatial resolution; description and in order of increasing wavelength, they are as follows: (1; 645nm; 250m; red), (2; 853nm; 250m; reflective IR), (3; 469nm; 500m; blue), (4; 555nm; 500m; green), (26; 1.38mm; 1km; short- wave water vapor), (31; 11.0mm;

1km; IR clean window), and (32, 12.0mm 1km; IR dirty window). The over-water algorithm, uses MODIS channels 2, 3, and 4, and the over-land, algorithm enlists all seven channels listed above.

### 3.1. Dust enhancement

Dust in atmosphere is usually associated with clouds, smoke, sea salt, pollutants, background etc. Dust detection requires separation of dust from these associates. Dust enhancement uses various techniques like color composites, ratioing, Normalized Difference Dust Index and various combinations of Visible/Near-Infra-Red (VNIR), Thermal-Infra-Red (TIR) band to separate associates and enhance the dust by using hydra software.

True color composite 1(R), 4(G), 3(B) with 250m spatial resolution, is generated for the dust enhancement and detection (Fig. 2 a & c). Using a tri-spectral technique (Ackerman, 1997) pseudo color composite is made with band combination 20(R), 1(G), 29(B) (Fig. 2 b & d). In the true color composite image, land, cloud, dust and sun glint region are seen in almost same color. Whereas, in pseudo color images, the land is seen pink and water is dark blue in color. Dust is seen yellow over land region and green over water surface (Fig. 2 d & b). The yellow colored dust is clearly distinguishable over pink land in pseudo color image. The smoke, dust particles and non-dust particles look alike and cannot be separated.

Thermal Infrared (TIR) have advantages as TIR data can be obtained during day or night, and can also be used on bright surfaces. Ackerman (1997) suggested a tri-spectral technique with imagery acquired at 29 (8.52nm, 1km), 31 (11.02, 1km), and 32 (12.03nm, 1km) to detect the dust storm characteristics. For the MODIS data, the brightness temperature at the wavelength of 11.03µm (T11) in channel 31 represents the dust storm top temperature and the brightness temperature at the wavelength of 12.02µm (T12) in channel 32 represents the temperature of the earth surface.

$$T12 - T11 (T12 - T11 \geq 1K) \text{ and } \Delta T = \begin{cases} 1 & (T12 - T11 \geq 1K) \\ 0 & (T12 - T11 < 1K) \end{cases} \text{ ----- (1)}$$

Generally, the  $\Delta T$  of dust region is more than 1 k, and  $\Delta T$  for the other object is less than 1k. So, the threshold of 1 k is used to separate the dust from other objects. The brightness temperature difference (BTD) method separates dust from clouds. Dust is less reflective than clouds in blue wavelengths (~0.47µm) and dust texture is more uniform than the texture of clouds (standard deviation of 3 × 3 pixels is less).

According to Miller's (2003), when dust is elevated from ground, it is cooler than the surroundings. This produces depressed IR brightness temperature against the hot skin temperature of the background land and can be easily detected. Dust has positive NDDI (Normalized Difference Dust Index) and clouds have negative NDDI value. NDDI is calculated as:  $NDDI = (R_{2.13 \mu m} -$

$$\begin{aligned} & R_{0.469 \mu\text{m}} / (R_{2.13 \mu\text{m}} + R_{0.469 \mu\text{m}}) \\ & = (b_7 - b_3) / (b_7 + b_3) \end{aligned}$$

NDDI is a very effective ratio for dust enhancement on land. It is not very suitable for dust over water as the reflectance of water is close to 0 in the 7th band. Therefore, this enhancement is used for separating clouds from dust only over the land. There is a very good contrast between brightness temperatures at 12  $\mu\text{m}$  and 11  $\mu\text{m}$  for dust over cool surface of water. The BTD (12, 11) is positive for dust. Thus, it is used to enhance dust over water.

### 3.2. Dust detection and mapping

The methodology used in this paper followed the procedure of Zhao et al., (2010) for dust detection and mapping. MODIS data from Terra (morning overpass) and/or Aqua (afternoon overpass) is suitable and is used. For processing MODIS data, the multispectral data analysis tool-kit HYDRA (HYperspectral data viewer for Development in Research Application) is used.

#### 3.2.1. Dust Detection over Ocean

To identifying suitable and good data, following procedures are carried out as described in Zhao et al., (2010).

Dust detection procedures:

There are three procedures for detecting dust over water. Any pixel that passes any of these three tests is flagged as dusty. Using Hydra software and respective bands (as described below) from MODIS data, dust detection is carried out.

- If  $BT_{11\mu\text{m}} - BT_{12\mu\text{m}} < 0.1\text{K}$  and  $-0.3 \leq NDVI \leq 0$ , then dust
- If  $R_{0.47\mu\text{m}}/R_{0.64\mu\text{m}} < 1.2$ , then dust
- If  $BT_{3.9\mu\text{m}} - BT_{11\mu\text{m}} > 10\text{K}$  &  $BT_{11\mu\text{m}} - BT_{12\mu\text{m}} < -0.1\text{K}$ , then dust

Where BT is brightness temperature (wavelength is given in subscript, e.g.,  $BT_{11\mu\text{m}}$ ), R is reflectance (wavelength is given in subscript, e.g.,  $R_{0.64\mu\text{m}}$ ) and  $NDVI = (R_{0.86\mu\text{m}} - R_{0.64\mu\text{m}}) / (R_{0.86\mu\text{m}} + R_{0.64\mu\text{m}})$ .

The thick dust over water is detected by adopting following procedure,

- $BT_{3.9\mu\text{m}} - BT_{11\mu\text{m}} > 20\text{K}$  (define potential thick dust regime)
- If  $BT_{11\mu\text{m}} - BT_{12\mu\text{m}} \leq 0\text{K}$  and  $-0.3 \leq NDVI \leq 0.05$  then thick dust.

The first part of the test associated with BTD is split window IR detection technique for thick dust. The second part of the test associated with NDVI is similar to the detection of non-thick dust

(Fig. 3a), which is used to reduce the false detection in the split window test (Zhao et al., 2010).

### 3.2.2. Dust Detection over Land

Following dust detection algorithm procedure is used for both dark and light surface desert area,

- If  $BT_{3.9\mu m} - BT_{11\mu m} \geq 25K$  then
- If  $MNDVI < 0.08$  &  $Rat_2 > 0.005$  then dust,

Where  $MNDVI = NDVI_2 / (R_{0.64\mu m} \times R_{0.64\mu m})$  and  $Rat_1 = (R_{0.64\mu m} - R_{0.47\mu m}) / (R_{0.64\mu m} + R_{0.47\mu m})$  and  $Rat_2 = (Rat_1 \times Rat_1) / (R_{0.47\mu m} \times R_{0.47\mu m})$ .

Dust reflects solar energy at  $3.9\mu m$  during the day, brightness temperature difference with  $BT_{11\mu m}$  is significant. Depending on the time of data acquisition, 25K threshold for the BTD (3.9, 11) is lowered down till 15K if the dust is not very dense. MNDVI (modified normalized difference index) gives a more accurate result in such case. MNDVI involves Red ( $\sim 0.64\mu m$ ) and reflective Infrared ( $\sim 0.86\mu m$ ) wavelengths. This is useful for detection of dust over semi-arid surface with small amounts of vegetation. Moreover dust absorbs blue ( $\sim 0.47\mu m$ ) wavelength. Therefore, the index  $Rat_2$  that is dependent on blue wavelength is used effectively.

To detect thick dust following algorithm is used,

- $BT_{11\mu m} - BT_{12\mu m} \leq -0.5K$  &  $BT_{3.9\mu m} - BT_{11\mu m} \geq 25K$
- &  $R_{1.38\mu m} < 0.035$
- $MNDVI < 0.2$

Higher threshold values are applied for separation of thick dust from the background (Fig. 3b). Therefore, satellite radiance measurements in these wavelengths show favorable results for dust detection (Fig. 3b). Dust absorbs more radiation at  $12\mu m$  than  $11\mu m$ , which causes BTD (11, 12) to become negative. The  $1.38\mu m$  channel is located in water vapor absorption band. If there are very dense clouds then, dust signature is picked up as clear sky.

The above procedures indicates that, the data satisfies all algorithms and the super sand storm is properly detected during its transport.

### 3.3. Super Sand Storm validation using CALIPSO LiDAR data

The Cloud-Aerosol Lidar and Infrared Pathfinder Satellite Observations (CALIPSO) satellite make continuous measurements of the Earth's atmosphere to retrieve the spatial and optical properties of clouds and aerosols from the CALIPSO Lidar backscatter data (Fig. 4a). CALIPSO

LIDAR Browse Images for Production Release [V3.20] were downloaded (Fig. 4b) from <http://www-calipso.larc.nasa.gov/products/lidar>. The footprint of CALIPSO overlaid over the MODIS scene to validate the presence of dust (Fig. 4c). In absence of any other CALIPSO data, a single footprint crossing sand storm towards eastern end (Fig. 4), provides significant information. The altitude of the dust storm is estimated from a profile of Total Attenuated Backscatter image and Vertical Feature Mask image (Fig. 4b). Both CALIOP profiles images (Fig. 4 c, d) confirms the existence of dust and helps in measuring altitude of the sand storm over the surface. Dense sand storm/aerosol over the Arabian Sea are seen floating from 500m to 3000m height, whereas, the clouds are seen floating between 7000m-13000m over the Arabian Sea during March 2012 event (Fig. 4b).

#### 3.4. Super Sand Storm migration monitoring

Aqua and terra MODIS scenes captured during 2<sup>nd</sup> half of March, 2012 were downloaded, enhanced, and processed using above stated methodology for detecting dust after eliminating unwanted associates like background, sun glint, cloud, smoke etc. The processed scenes were arranged date and time wise (Fig. 5). The scenes were geo-referenced and daily mosaics were prepared using Geographic Information System (GIS). The mosaic scenes were up-loaded on Google Earth. By adjusting optimum transparency, movements of the dust storm were monitored, with respect to location. The source, dust transport pathway and dissipation of the storm were deduced.

The dust/sand availability and wind direction and speed governs the migration of storm. Wind speed and direction depends upon temperature and pressure difference. Temperature and pressure differs as per height from the surface. Wind data at different pressure level for 3<sup>rd</sup> week of March 2012 (study period) available at ECMWF (<http://apps.ecmwf.int/datasets/>) were downloaded. Using FERRET software, wind speed, wind direction maps with respect to different pressure levels and time periods were prepared to recognize the possible storm pathway (Fig. 6)

HYSPLIT- Hybrid Single Particle Lagrangian Integrated Trajectory Model developed by Air Resources Laboratory of NOAA, USA was used for preparing backward trajectories maps to trace dust particles back to their source area. A matrix of points from 19<sup>o</sup> to 20<sup>o</sup> Latitude and 60<sup>o</sup> to 69<sup>o</sup> Longitudes within study area is considered for drawing backward trajectory maps. Archived meteorological file named “gdas.1 mar12.w3” containing meteorological data of 3<sup>rd</sup> week of March 2012 was used to draw backward trajectory maps for four different times of the day, for the event days. In addition, backward and forward trajectories with respect to several other locations along possible pathway for different days and time were studied to understand storm movement. A few back trajectories are displayed (Fig. 7).



#### 4. Results

After analyzing relevant MODIS day-night images for 2<sup>nd</sup> half of March 2012, it was deduced that the Super Sand Storm was resulted from the convergence of two different storms. The first front carried dust from Syria-Iraq and Kuwait, and the second front stirred dust in Iran-Afghanistan-Pakistan border. The storm (first front) formed along the Syria-Iraq border on March 17 (Aqua satellite observation). The dust plumes that blew across Syria and Iraq arose from Southeast of the Buhayrat al Asad (also known as Lake Assad) reservoir, rocky desert covers large stretches of Syria (Fig. 5a), which is a source points in this region. Winds carried the dust toward the southeast, and the storm picked up more fine sediments across Iraq. Fine sediments from the Tigris and Euphrates Riverbeds in Iraq and vast sand seas in Saudi Arabia provided plentiful material for dust storms (Fig. 5b). The dust storm continued its southward movement for two more days, drifting off the southern end of the Arabian Peninsula and over the Gulf of Aden. This dust storm may be connected to a local phenomenon known as the “Shamal” (an Arabic word for “north”). A Shamal is defined as sustained winds of 25 knots or greater. Wind direction is almost always northwesterly. The winter Shamal is generally characterized by durations of either 24-36 hours or 3-5 days. A sketch of possible pathways of sand storms is shown (Fig.8).

On March 19, 2012, the MODIS on Terra satellite captured a storm (second front) sweeping across Iran, Afghanistan, and Pakistan. Source points were located (Fig. 5c) as combination of sand seas and impermanent lakes occur along the borders between Iran, Pakistan, and Afghanistan, and the fine sediments provided material for dust storms. Westerly Shamal winds pushed dust storm westerly and southwesterly. While migrating, on 20<sup>th</sup> March, storm deposited the dust in the southern Iran, UAE, Oman, Yemen and Saudi Arabia (Fig. 5d). In Saudi Arabia, advancement of Cold-Front towards the south-east direction resulted into the upsurge the amount of dust over the Arabian Sea.

In India, a system of two low pressures has pulled the wind and subsequently the dust plume. One low pressure was located offshore Goa-Karnataka border while the other one is over the North-East part of Central India (IMD, 2012) which has pulled an arm of the dust storm (a plume) towards west coast of India across Arabian Sea (5e, f) and has also caused advancement of the plume in Central India (Fig. 5g). On 24<sup>th</sup> March the dust storm dissipated over Bay of Bengal region (Fig. 5h).

Dust storm migration was studied in light of existing wind pattern, Calipso images and backward trajectories. Data for these three variety was collected on 20<sup>th</sup> March 2012 at 23:00 hrs. Wind patterns only on 19 and 20 of March indicates wind direction towards south in northern Arabian Sea from surface to 1000mb pressure level (110.8m) (Fig. 6). Above 1000mb pressure level

(110.8m), the anti-cyclonic wind pattern was noted at various heights over Arabian Sea during 3<sup>rd</sup> week of March 2012 (Fig. 9).

The backward trajectory drawn from matrix situated within sand storm area at 500m height indicate sand source as the north-eastern Iraq and partly as south Iraq (Fig. 7a). Dust/sand is transported from the source to North Arabian Sea after crossing 2000m high terrain. The backward trajectory drawn from the same matrix at 1000m height indicate source to the west, from Gulf of Oman and Persian Gulf and beyond (Fig. 7b). The backward trajectory drawn from height 2000m and 3000m indicate similar source and exhibit impact of anticyclone on trajectories (Fig. 7c, d). All these back trajectories are calculated for 48 to 72 hrs.

#### 4.2. Sea Surface Temperature and Chlorophyll *a* analysis

Sea Surface Temperature and Chlorophyll *a* concentration data for March 17<sup>th</sup> to 31<sup>st</sup> are Standard Mapped Image (SMI) products observed by the MODIS/AQUA with spatial resolution of 4×4 km. To study Sea Surface Temperature and chlorophyll *a* concentration variability in the Arabian Sea during the event, daily image, three day composite and eight day composite level 3 binned data were downloaded from MODIS web site (<http://oceancolor.gsfc.nasa.gov>). The SST and Chlorophyll *a* data were analyzed using SEADAS image analysis package and daily, 3 day composite and 8 day composite images were generated. Daily and 3 day composite images were studied to understand variability of SST and Chlorophyll *a*. Composite images of 8 days data provided comprehensive picture of weekly variability (Fig. 10, 11, 12).

While analyzing daily composite, 3 day composite and 8 day composite of day time images of SST, it was noted that SST lowered from 17<sup>th</sup> March to 20<sup>th</sup> March (Fig. 10) and SST showed increasing trend from 21<sup>st</sup> to 24<sup>th</sup> of March. Similar trend was observed while analyzing SST images captured during night (Fig. 11). Chlorophyll variability study from daily composite, 3 day composite and 8 day composite of day and night indicated that high chlorophyll *a* concentration reduced from 17<sup>th</sup> March to 20<sup>th</sup> March. Chlorophyll concentration decreased up to 22<sup>nd</sup> March in the northern Arabian Sea and afterwards the chlorophyll concentrations increased to more than 10 mg/m<sup>3</sup> in the western part of Arabian Sea along the Oman and Yemen coastal region (Fig. 12).

### 5. Discussion and conclusion

Dust storm detection: As the spectral properties of dust aerosol are different from ground or sea, some predefined thresholds for various linear combinations can make dust clearly visible in the scene. NDDI and BTM (11, 12) are effective techniques for dust detection over land and over ocean, respectively. The algorithms discussed in this study is demonstrated by daytime images of Aqua and

Terra MODIS only. However, the same methods can be applied with any other multi-channel satellite data with proper or same channels as used in this study. Cirrus clouds may produce some false positive results. Due to relatively weak aerosol signal and presence of bright land surface, thin and widely dispersed dust plumes may be missed in the detection process. For better classification accuracy, the results are validated by CALIPSO LiDAR measurements.

The results of this study have been evaluated by comparing values of linear combinations of MODIS channels with CALIOP measurements to minimize the misclassification. As the footprint of CALIOP is very narrow, it may miss the dust event by hundreds of kilometers at given time. However, as Aqua MODIS and CALIPSO are part of the same A-Train, there are high prospects of getting sufficient data for this type of comparison.

Sand storm path-way determination: As per first hypothesis, this storm resulted from the convergence of two different storms. The first front carried dust from Syria-Iraq and Kuwait, and the second front stirred dust in southeastern Iran. Both the sand storms converge in southern Saudi Arabia with huge outbreak of sand. The clash coincided with cold front driven by the Shamal wind towards the south-east direction resulted into the upsurge the amount of dust over the Arabian Sea. To the East coast of Arabian sea, in India, due to development of low pressure area, during 19<sup>th</sup> to 21<sup>st</sup> of March (IMD report 2012), an arm of the dust storm (a plume) was pulled towards west coast of India across Arabian Sea and has also caused advancement of the plume in Central India. The daily average wind data of 19<sup>th</sup> and 20<sup>th</sup> March support the migration of the storm (Fig. 6b).

During this period, India was under the influence of this severe dust storm and the MODIS observed Aerosol Optical Difference (AOD) is about 0.9 -1.0 in the northern India. Due to the presence of anticyclone in the Arabian Sea (Harikrishnan et al., 2012), the transport of dust to the southern peninsula was delayed. The shadow band radiometer measurements at northern region (Pune) showed drastic increase in AOD up to 0.7 (500 nm) on 22nd and 23rd March due to the dominance of dust component. Due to this dust loading, solar dimming observed at the surface from the ground measurements is  $\sim 300$  W/m<sup>2</sup>. The radioactive forcing is derived about  $\sim -32$  W/ m<sup>2</sup> from the surface and  $\sim 15.98$  W/m<sup>2</sup> at the top of the atmosphere (Harikrishnan et. al. 2012).

Another school of thought (Sathiyamoorthy 2012) suggests that the convergence of the two sand storms and extending sand storm plume across the Arabian Sea, are two independent events. Strong surface pressure gradient over Baluchistan/Afghanistan (Fig. 5c) associated with the passing of a western disturbance caused strong winds (Fig. 5d). This caused dust storm over Baluchistan, Afghanistan and Iran on the evening of 19 March 2012. The dust migrated south/southeastward

along with the prevailing wind, reached south of 20°N, by forming sand storm plume across Arabian Sea (Fig. 5e, f) and Northern states of India by 20 March 2012 (Fig. 13a). On 21 March 2012, dust further spread south/southeast ward pushing the plume southwards (Fig. 5g) beyond 25°N and covering parts of Central India (Fig. 13b). As per daily average wind map, wind direction on 19<sup>th</sup> and 20<sup>th</sup> is towards south (Fig. 6e-h) and backward trajectory up to 1000m height (Fig. 7A) support the above hypothesis. However, above 1000mb pressure level, winds flow from west to East in an anti-cyclonic manner (Fig. 6 a-d) and backward trajectories (Fig. 7 b-c) also indicate source of dust/sand as Saudi Arabia. Hence from available data, it may be concluded that supper sand storm migration over Arabian Sea took place according to either hypothesis. Storm followed Southward migration as per 2<sup>nd</sup> hypothesis up to 1000mb pressure level, whereas, as per first hypothesis, two storm fronts collided with cold front heading south eastward tossed the large amount of dust over the Arabian Sea. Development of low pressure area, during 19<sup>th</sup> to 21<sup>st</sup> of March (IMD report 2012), and anticyclone winds over the study area, pulled the dust/sand eastwards towards west coast of India across Arabian Sea above 1000mb pressure level. The anti-cyclonic winds in 600mb pressure level (4204.7 m height) (Fig. 9), suppressed the sand/dust southwards to Arabian Sea. Either hypothesis cannot be confirmed due limited availability of field measurements, and remote sensing data.

The Arabian Sea receives a relatively large supply of mineral matter dust from the arid land-masses bordering it to its northern part. The deposition of atmospheric dust and its partial dissolution in seawater is one of the key processes influencing the cycling of Al, Fe in the ocean (Maring and Duce 1987; Gehlen et al., 2003; U. Schu"X ler et al., 2005). During the present event also dust deposition has taken place. However, unless pre and post event volumes of the dusts are known, dust deposited in Arabian Sea cannot be predicted. Post event increase in chlorophyll\_a concentration (Fig. 12) indicates deposition of iron laden dust in Arabian Sea. It is also true that dust deposition can easily be mistakenly attributed as a primary cause of enhanced biological activity and that, due to the slow dissolution of iron, dust-mediated phytoplankton blooms are probably rare in the modern ocean (Boyd et al., 2010).

Sediments are the ultimate sinks for atmospherically derived mineral dust. Dust deposition supply iron as a micronutrient to Fe-limited waters, thereby fertilizing phytoplankton productivity (Martin et al., 1991; Jickells et al., 2005; Wolff et al., 2006; Boyd and Ellwood 2010). Increased productivity results in drawdown of atmospheric CO<sub>2</sub>; subsequent export of biogenic carbon from surface to deep ocean waters can lead to long-term geological sequestration of carbon (Martinez-Garcia et al., 2009). It is therefore well established that aeolian dust responds to, and has a direct role in, climate change (Jickells et al., 2005; Maher et al., 2010).

From on-going discussion is concluded that 1. NDDI and BTM (11, 12) are effective techniques for dust enhancement over land and over ocean, respectively. 2. Zhao et al., (2010) procedures are suitable for dust detection over land and ocean. 3. CALIPSO data, if available for event, confirms presence and provides vertical dimension of dust storm. 4. The combination of both suggested hypothesis provides acceptable explanation for large scale migration of Super Dust Storm across the Arabian Sea and south-east Asian region. 5. SST is lowered during the event and chlorophyll *a* concentration is increased during post event period.

The present study demonstrates usage of remote sensing data and geospatial techniques in detecting and mapping of dust events and monitoring dust transport along specific regional transport pathways over land and ocean. It also suggest source regions of individual dust events.

In future, it is necessary to carry forward such study to identify the role of dust in 1) biogeochemical cycles and in soil formation, 2) to understand the possible role that dust may have played in Pleistocene climatic changes, and 3) to know impact of dust storms upon human health in a variety of ways.

**Acknowledgements:** We express our sincere gratitude to Director, National Institute of Oceanography for permitting us to publish this material. MODIS data was accessed from <http://modis.gsfc.nasa.gov/> web page. This is NIO contribution number .....

## References

- Ackerman, S.A., 1997. Remote Sensing aerosols using satellite infrared observation. *J. Geophys. Res.* 102, 17069-17079.
- Alpert, P., Kishcha, P., Shtivelman, A., Krichak, S.O., Joseph, J.H., 2004. Vertical distribution of Saharan dust based on 2.5-year model predictions. *Atmos. Res.* 70, 109–130.
- Antoine, D., Nobileau, D., 2006. Recent increase of Saharan dust transport over the Mediterranean Sea, as revealed from ocean color satellite (SeaWiFS) observations. *J. Geophys. Res.* 111, D12214.
- Baddock, M.C., Bullard, J.E., Bryant, R.G., 2009. Dust source identification using MODIS: a comparison of techniques applied to the Lake Eyre Basin, Australia. *Remote Sens. Environ.* 113, 1511–1528.
- Badarinath, K.V.S., Kharol, S.K., Kaskaoutis, D.G., Sharma, A.R., Ramaswamy, V., Kambezidis, H.D., 2010. Long-range transport of dust aerosols over the Arabian Sea and Indian region — A case study using satellite data and ground-based measurements. *Global and Planetary Change.* 72, 164–181.
- Banks, J.R., Brindley, H.E., Flamant, C., Garay, M.J., Hsu, N.C., Kalashnikova, O.V., Klüser, L., Sayer, A.M., 2013. Intercomparison of satellite dust retrieval products over the West African Sahara during the Fennec campaign in June 2011. *Remote Sens. Environ.* 136, 99-116.

- Boccone, M., 2010. Dust detection algorithm using MODIS data and hydra software. Present Environment and sustainable development. NR. 4, 75-90.
- Boyd, P.W., Ellwood, M.J., 2010. The biogeochemical cycle of iron in the ocean. *Nat. Geosci.* 3, 675–682.
- Boyd, P.W., Mackie, D.S., Hunter, K.A., 2010. Aerosol iron deposition to the surface ocean - Modes of iron supply and biological responses. *Marine Chemistry*. 120, 128–143.
- Bullard, J., Baddock, M., McTainsh, G., Leys, J., 2006. Sub-basin scale dust source geomorphology detected using MODIS. *Geophys. Res. Lett.* 35(15), L1504.
- Choobari, O.A, Zawar-Reza, A., Sturman, A., 2014. The global distribution of mineral dust and its impacts on the climate system: A review. *Atmos. Res.* 138, 152-165.
- Engelstaedter, S., Tegen, I., Washington, R., 2006. North African dust emissions and transport. *Earth-Science Reviews* 79(1–2), 73–100.
- Gao, H., Washington, R., 2009. The spatial and temporal characteristics of TOMS AI over the Tarim Basin, China. *Atmos. Environ.* 43(5), 1106-1115.
- Gehlen, M., Heinze, C., Maier-Reimer, E., Measures, C.I., 2003. Coupled Al–Si geochemistry in an ocean general circulation model: a tool for the validation of oceanic deposition fields? *Global Biogeochemical Cycles*. 17, 1028.
- Goudie, A.S., Middleton, N.J., 2001. Saharan dust storms: nature and consequences. *Earth-Science Reviews*. 56, 179-204.
- Guo Ni and Liang Yun, 2006. A study on quantitative identification of sand and dust storm using MODIS data. *Arid Meteorology*. 24(1), 1-5.
- Harikishan, G., PadmaKumari, B., MaheshKumar, R.S., 2012. Impact of intense dust storm of March 2012 on surface reaching solar radiation over Pune, in: *Proc. IASTA-2012/ SESSION-IV /P-047, Pub.:* Indian Aerosol Science and Technology Association, Bhabha Atomic Research Centre, Mumbai, India, pp. 299-300.
- Huang, J., Minnis, P., Lin, B., Wang, T., Yi, Y., Hu, Y., 2006. Possible influences of Asian dust aerosols on cloud properties and radiative forcing observed from MODIS and CERES. *Geophys. Res. Lett.* 33, L06824.
- Ichoku, C., Kaufman, Y.J., Remer, L.A., Levy, R., 2004. Global aerosol remote sensing from MODIS. *Advance Space Research*. 34, 820-827.
- IMD report, 2012. Indian Daily Weather report 16-31 March 2012. All India weather report, Indian Meteorological department.
- Isaacman, A., Toller, G., Guenther, B., Barnes, W.L., Xiong, X., 2003. MODIS Level 1B Calibration and Data Products. *Proceedings of SPIE*, 5151, 552-562.
- Jickells, T.D., An, Z.S., Andersen, K.K., Baker, A.R., Bergametti, G., Brooks, N., Cao, J.J., Boyd, P.W., Duce, R.A., Hunter, K.A., Kawahata, H., Kubilay, N., laRoche, J., Liss, P.S., Mahowald, N., Prospero, J.M., Ridgwell, A.J., Tegen, I., Torres, R., 2005. Global iron connections between desert dust, ocean biogeochemistry, and climate. *Science*. 308 (5718), 67–71.
- Kaskaoutis, D.G., Kambezidis, H.D., Nastos, P.T., Kosmopoulos, P.G., 2008. Study on an intense dust storm over Greece. *Atmos. Environ.* 42, 6884–6896.

- Kaufman, Y.J., Tanre, D., Boucher, O., 2002. A satellite view of aerosols in the climate system. *Nature*. 419 (6903), 215–223.
- Liss, P.S., Turner, S.M., 2000. The influence of iron on ocean biology and climate: insights from the IronEx studies in the Equatorial Pacific, in: Hanson RB, Ducklow HW and Field JG (Eds.), *The changing Ocean Carbon Cycle. A Midterm Synthesis of joint Global Ocean Flux Study*. Pub: Cambridge University Press, Cambridge.
- Liu, D., Wang, Z., Liu, Z.Y., Winker, D., Trepte, C., 2008. A height resolved global view of dust aerosols from the first year CALIPSO lidar measurements. *J. Geophys. Res-Atmos.* 113, art.no. D16214.
- Maher, B.A., Prospero, J.M., Mackie, D., Gaiero DHesse, P.P., Balkanski, Y., 2010. Global connections between aeolian dust, climate and ocean biogeochemistry at the present day and at the last glacial maximum. *Earth-Science Reviews.* 99, 61–97.
- Maring, H.B., Duce, R.A., 1987. The impact of atmospheric aerosols on trace metal chemistry in open ocean surface seawater, aluminium. *Earth and Planetary Science Letters.* 84, 381–392.
- Martin, J.H., Gordon, R.M., Fitzwater, S.E., 1991. The Case for Iron. *Limnology and Oceanography.* 36(8), 1793–1802.
- Martinez-Garcia, A., Rosell-Mele, A., Geibert, W., Gersonde, R., Masque, P., Gaspari, V., Barbante, C., 2009. Links between iron supply, marine productivity, sea surface temperature, and CO<sub>2</sub> over the last 1.1 Ma. *Palaeoceanography.* 24, PA1207.
- Miller, S.D., 2003. A consolidated technique for enhancing desert dust storms with MODIS. *Geophys. Res. Lett.*, 30, 2071-2074.
- Nishihama, M., Wolfe, R.E., Fleig, A.J., Blanchette, J., Kuyper, J., 2000. MODIS Geolocation Algorithm and Error Analysis Tools. *IEEE Trans. Geosci. Remote. Sens.*, 5, 2053-2055.
- Papadimas, C.D., Hatzianastassiou, N., Mihalopoulos, N., Querol, X., Vardavas, I., 2008. Spatial and temporal variability in aerosol properties over the Mediterranean basin based on 6 yr (2000–2006) MODIS data. *J. Geophys. Res.* 113, D11205.
- Redmond, H.E., Dial, K.D., Thompson, J.E., 2010. Light scattering and absorption by windblown dust: Theory, measurement, and recent data. *Aeolian Research.* 2(1), 5-26.
- Sathiyamoorthy, V., 2012. Dust storm conditions in March 2012 from satellite imagery and NCEP. Megha - world Meteorological Day Issue, Indian Meteorological Society, Ahmadabad Chapter, Jan-March, 2012.
- Schepanski, K., Tegen, I., Laurent, B., Heinold, B., Macke, A., 2007. A new Saharan dust source activation frequency map derived from MSG-SEVIRI IR channels. *Geophys. Res. Lett.* 34, L18803.
- Slingo, A., Ackerman, T.P., Allan, R.P., Kassianov, E.I., McFarlane, S.A., Robinson, G.J., Barnard, J.C., Miller, M.A., Harries, J.E., Russell, J.E., Dewitte, S., 2006. Observations of the impact of a major Saharan dust storm on the atmospheric radiation balance. *Geophys. Res. Lett.* 33, L24817, 1-5.
- Schuler Uwe, Balzer Wolfgang, Deeken Aloys, 2005. Dissolved Al distribution, particulate Al fluxes and coupling to atmospheric Al and dust deposition in the Arabian Sea. *Deep-Sea Research II.* 52, 1862–1878.
- Tegen, I., 2003. Modeling the mineral dust aerosol cycle in the climate system. *Quaternary Science Reviews.* 22, 1821–1834.

- Vachon, P., Rayol, A., Aubé M., Toubbé B., O'Neill, N.T., 2004. Remote sensing of aerosols over North American land surfaces from POLDER and MODIS measurements. *Atmos. Environ.* 38(21), 3501-3515.
- Vaughan, M., Young, S., Winker, D., Powell, K., Omar, A., Liu, Z., Hu, Y., Hostetler, C., 2004. Fully automated analysis of space-based lidar data: an overview of the CALIPSO retrieval algorithms and data products. *Laser Radar Techniques for Atmospheric Sensing*, in: Upendra N. Singh (Eds.), *Proceedings of SPIE Vol. 5575* (SPIE, Bellingham, WA, 2004).
- Washington, R., Todd, M., Middleton, N., Goudie, A.S., 2003. Global dust storm source areas determined by the total ozone monitoring spectrometer and ground observations. *Ann Assoc Am Geogr.* 93,297–313. Published by Blackwell Publishing, 350 Main Street, Malden, MA 02148, and 9600 Garsington Road, Oxford, OX4 2DQ, UK.
- Wolff, E.W., Fischer, H., Fundel, F., Ruth, U., Twarloh, B., Littot, G.C., Mulvaney, R., Rothlisberger, R., de Angelis, M., Boutron, C.F., Hansson, M., Jonsell, U., Hutterli, M.A., Lambert, F., Kaufmann, P., Stauffer, B., Stocker, T.F., Steffensen, J.P., Bigler, M., Siggaard-Andersen, M.L., Udisti, R., Becagli, S., Castellano, E., Severi, M., Wagenbach, D., Barbante, C., Gabrielli, P., Gaspari, V., 2006. Southern Ocean sea-ice extent, productivity and iron flux over the past eight glacial cycles. *Nature.* 440 (7083), 491–496.
- Yingjie Li, Yong Xue, Gerrit de Leeuw, Chi Li, Leiku Yang, Tingting Hou, Farhi Marir, 2013. Retrieval of aerosol optical depth and surface reflectance over land from NOAA AVHRR data. *Remote Sens. Environ.* 133, 1-20.
- Zhao Tom X-P, Ackerman Steve, Guo Wei, 2010. Dust and Smoke Detection for Multi-Channel Imagers. *Remote Sensing* 2, 2347-2368.



## FIGURE CAPTIONS

- Fig. 1. MODIS AQUA image covering study area is overlapped on Google Earth Image.
- Fig. 2. Dust storm over Ocean (a) true color RGB image, (b) pseudo color RGB image and over land area (c) true color RGB image, (d) pseudo color RGB image.
- Fig. 3a. Scatter plot of brightness temperature difference and reflectance  $BT_{11\mu m} - BT_{12\mu m} \leq -0.5K$  &  $BT_{3.9\mu m} - BT_{11\mu m} \geq 25K$  &  $R_{1.38\mu m} < 0.035$  algorithm.
- Fig. 3b. Scatter plot of brightness temperature difference, NDVI and reflectance using algorithm  $((R_7 - R_3) / (R_3 + R_7)) \geq 0.0$  and  $BT(32) - BT(31) \geq 0.0$ .
- Fig. 4. a) CALIPSO path crossing study region, b) Vertical Feature Mask (VFM) along CALIPSO path, c) Footprint of CALIPSO on the MODIS scene, d) MODIS image of study region showing CALIPSO path.
- Fig. 5. Storm migration pathway of Super Sand Storm derived from successive MODIS images.
- Fig. 6. Image showing daily average wind speed & direction pattern on 20<sup>th</sup> March 2012 at different pressure levels (a) 700 (b) 850 and (c) 600 mbs.
- Fig. 7. The backward trajectory drawn from matrix of points from 19<sup>o</sup> to 20<sup>o</sup> N Latitude and 60<sup>o</sup> to 69<sup>o</sup> E Longitudes situated within sand storm area at (a) 500m, (b) 1000m, (c) 2000m, and (d) 3000m height indicate sand source for Super Sand Storm.
- Fig. 8. Surface wind at 10m height from March 18- March 21.
- Fig. 9. Surface pressure over the study region from March 18- March 21.
- Fig. 10. Plots showing (a) 200 hpa wind speed, (b) 850hpa and (c) 700hpa pressure heights from March 18-March 21.
- Fig. 11. Latitudinal vertical cross section from 1000 to 10 hpa of zonal wind speed in m/s for the period of March 18-March 21.
- Fig. 12. Sketch shows pathways of sand storms, location of cold front and low pressure belt. Thin arrows indicate pathway of one dust storm, red arrows indicate pathway of second storm and thick arrows indicate direction of an arm of the dust storm pulled due to low pressure formation. Spot surrounding circle indicate source of the storms.
- Fig. 13. Represent the eight days composite of sea surface temperature detected by sensors onboard aqua and terra satellites during day time.
- Fig. 14. Represent the eight days composite of Chlorophyll a detected by sensors onboard aqua and terra satellites during day time.
- Fig. 15. Chlorophyll\_a concentration (mg/m<sup>3</sup>) in a box average area (58<sup>o</sup>E-62<sup>o</sup>E, 18<sup>o</sup>E-22<sup>o</sup>N) during the month of event.
- Fig. 16. Satellite images (a, b) taken on 20<sup>th</sup> and 21<sup>st</sup> March 2012 by Kalpana 1, Meteorological satellite of Indian Space Research Organization, c) Mean sea level pressure on 19<sup>th</sup> March 2012, and d) Surface winds (m/s) measured on 19<sup>th</sup> March 2012 at 1800 UTC.

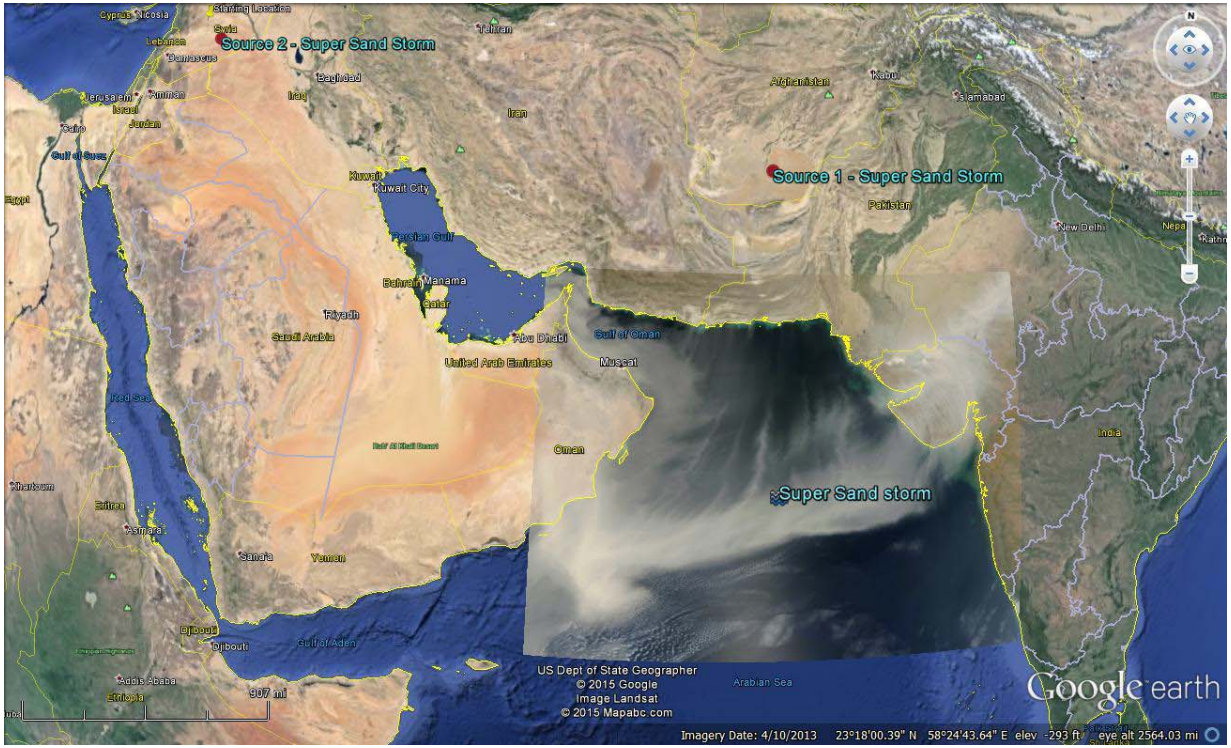


Figure 1

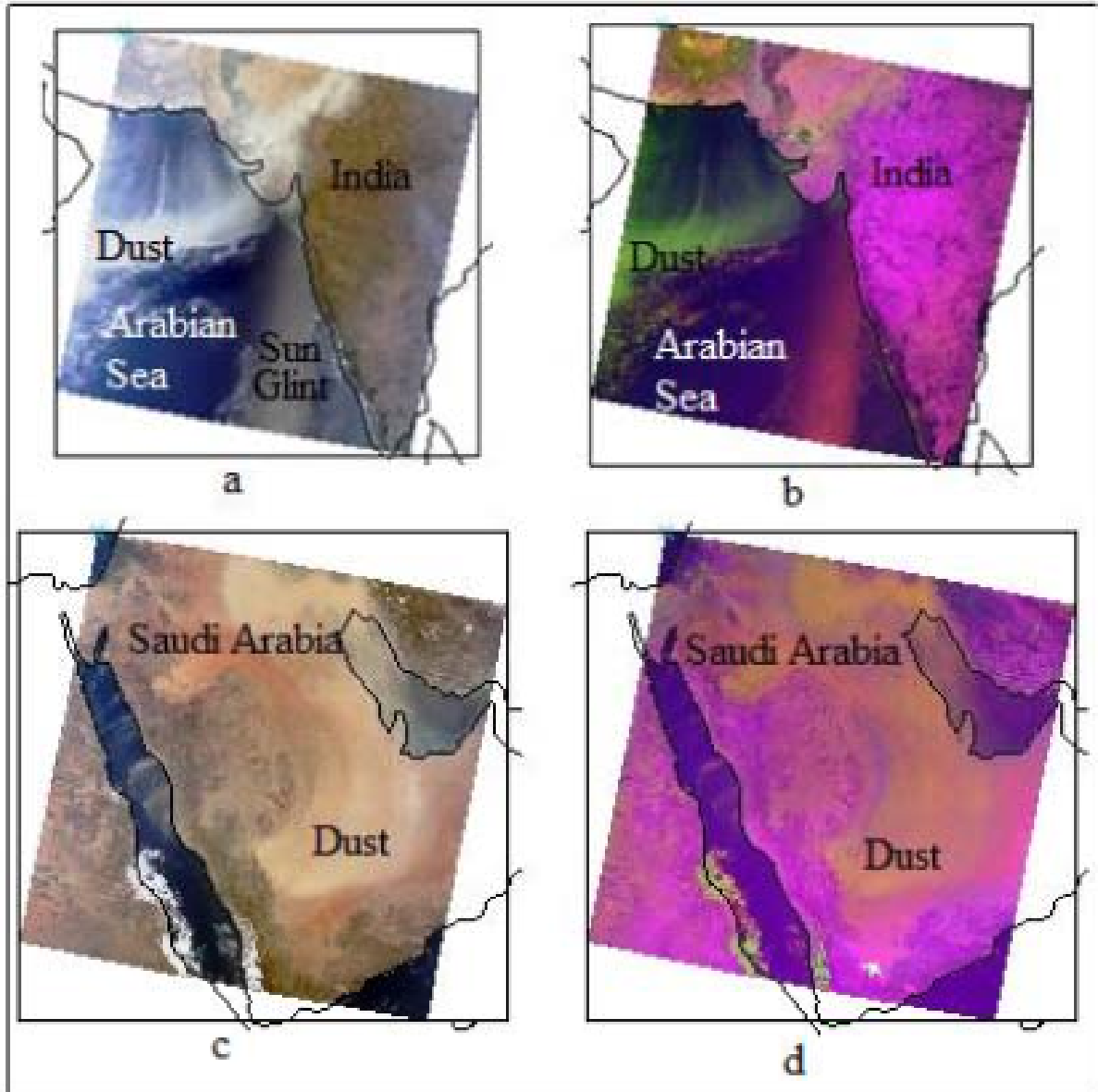
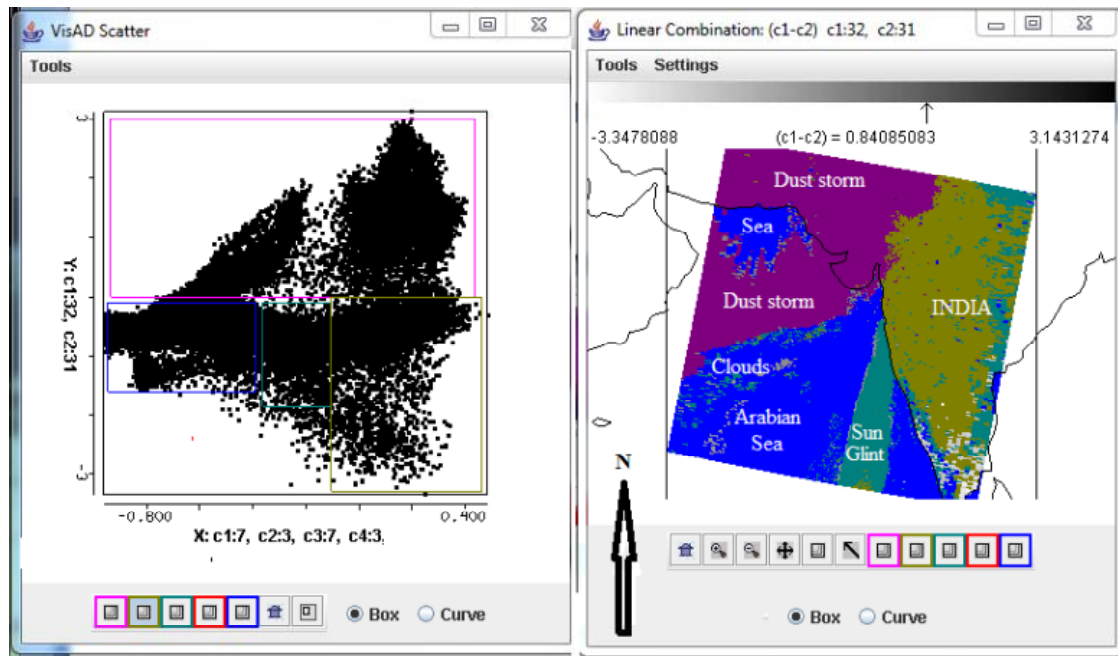
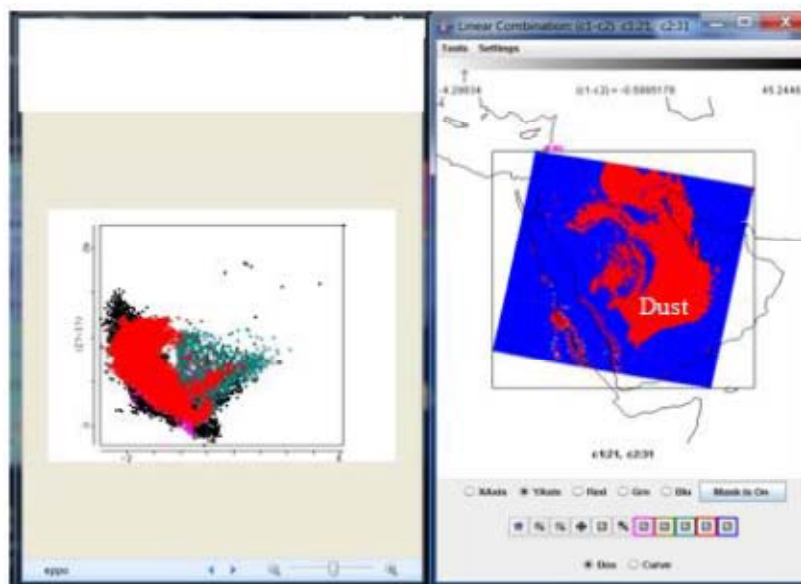


Figure 2



3a



3b

Figure 3

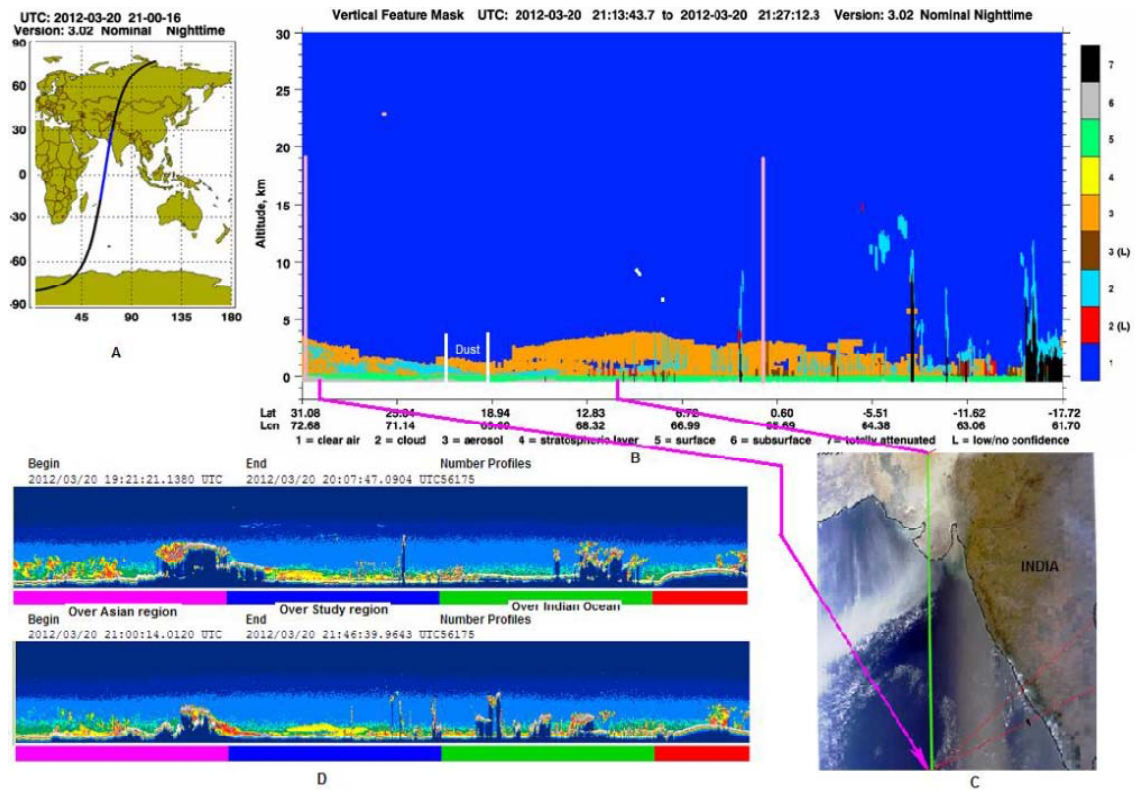


Figure 4

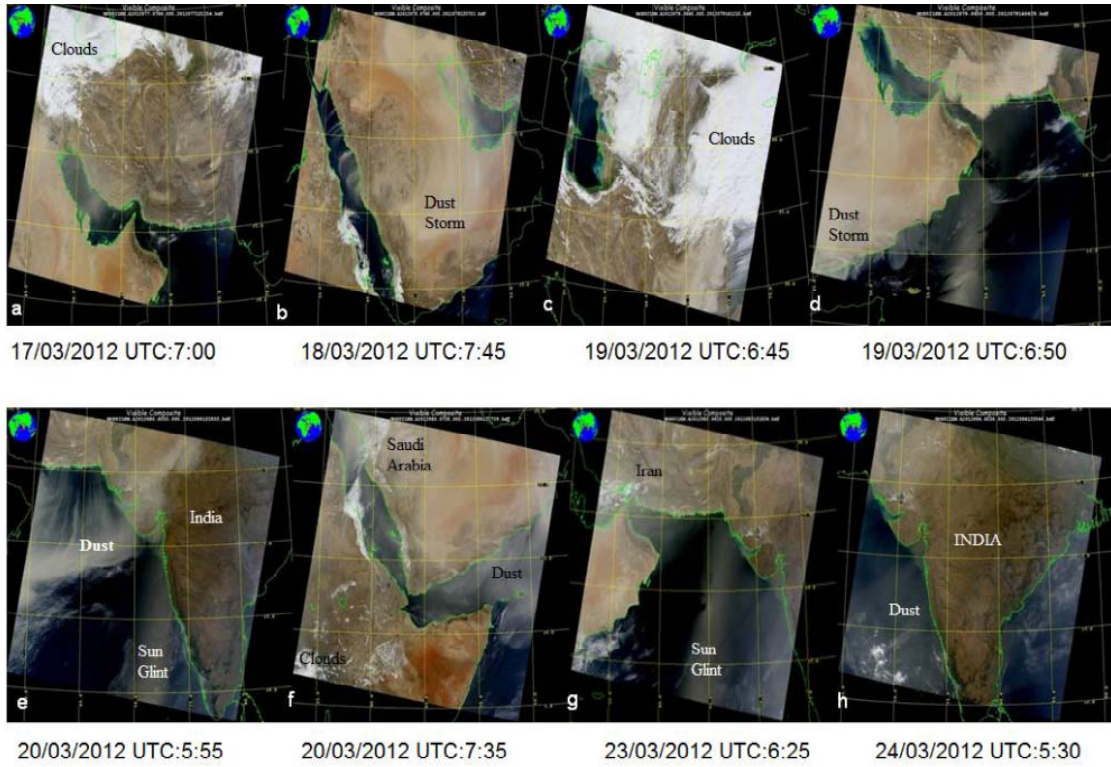


Figure 5

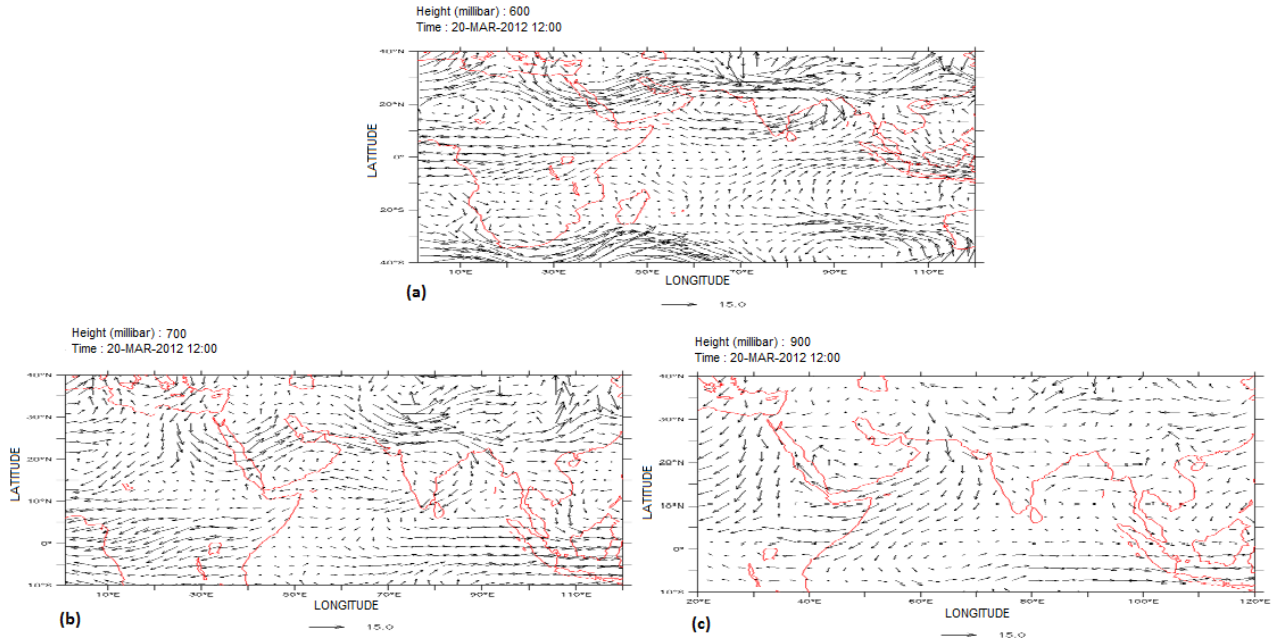


Figure 6

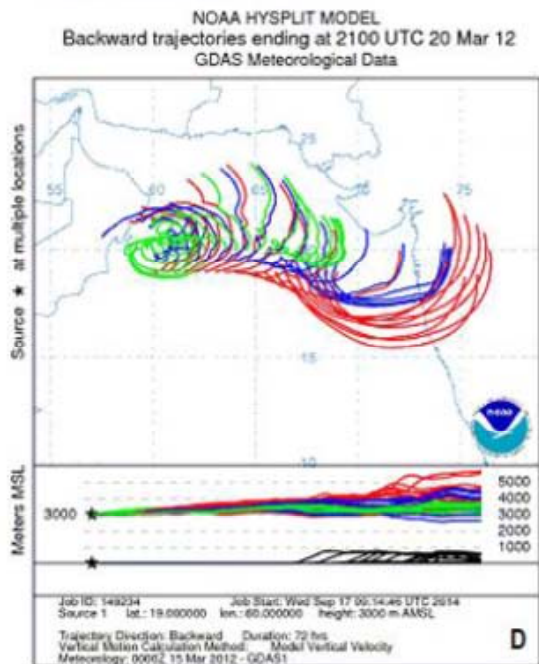
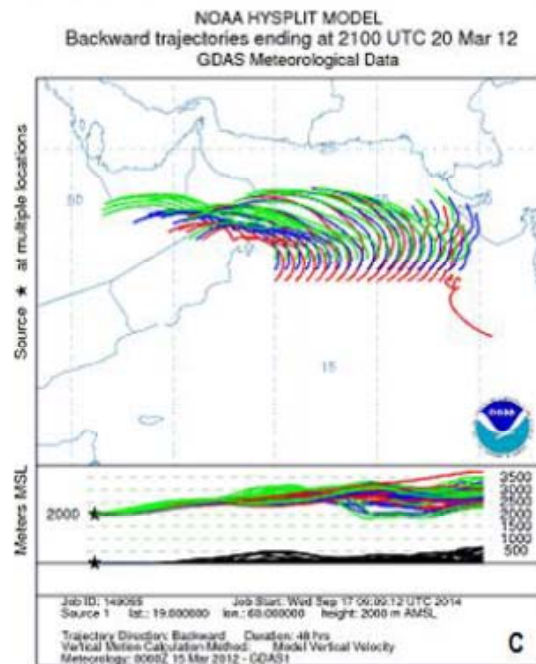
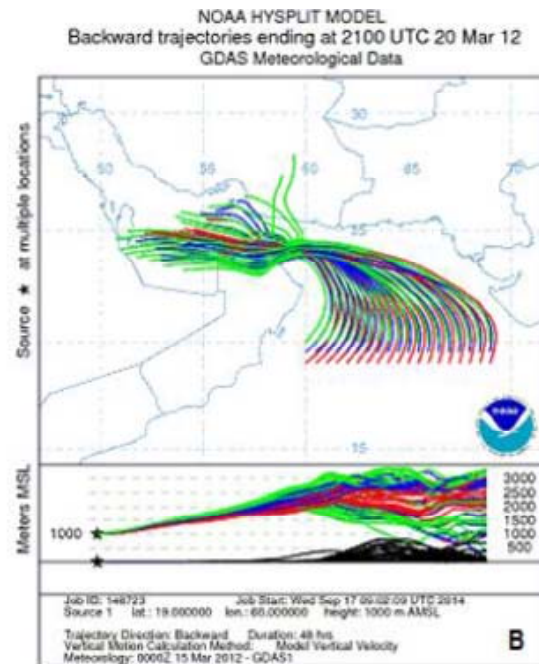
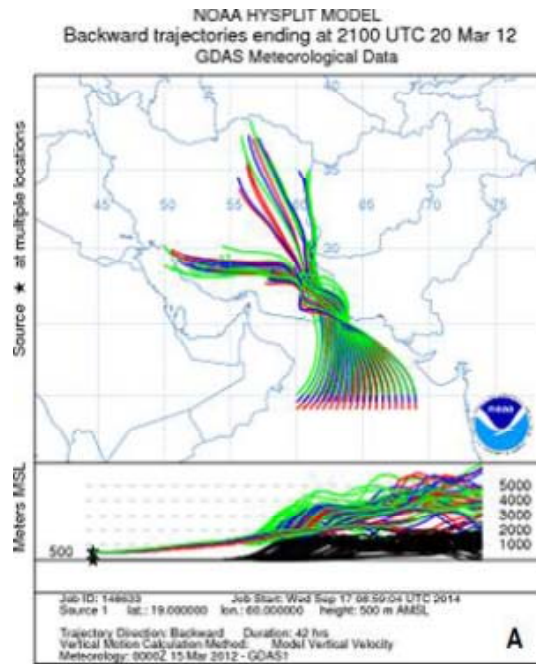


Figure 7



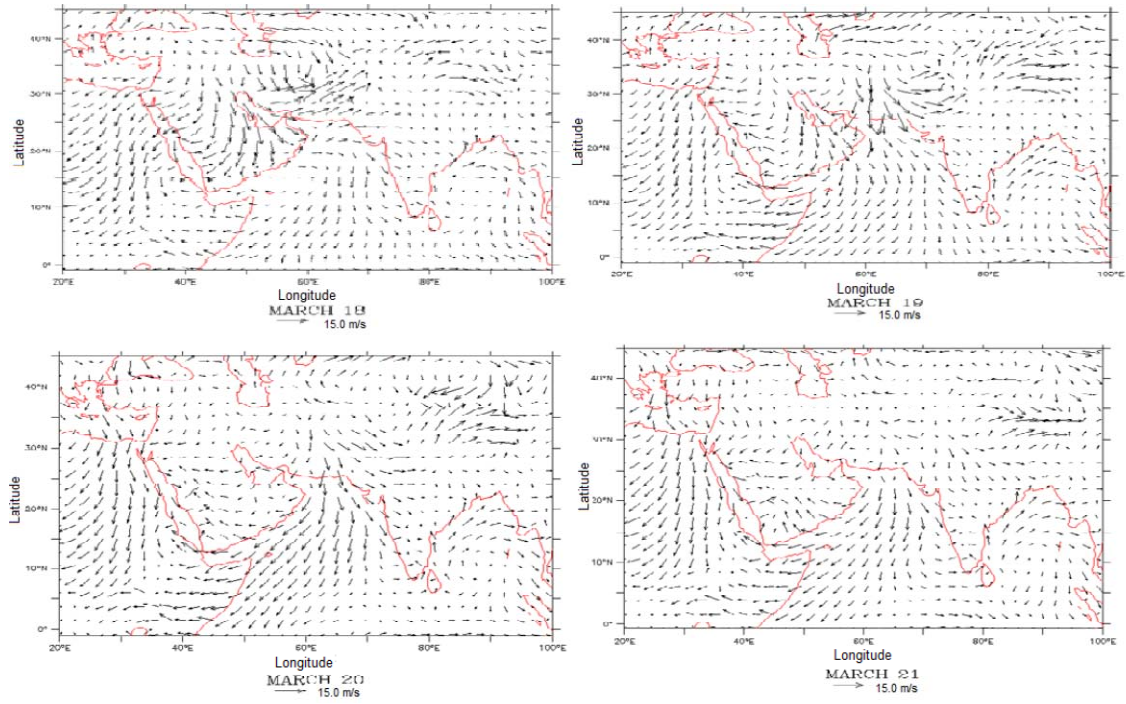


Figure 8

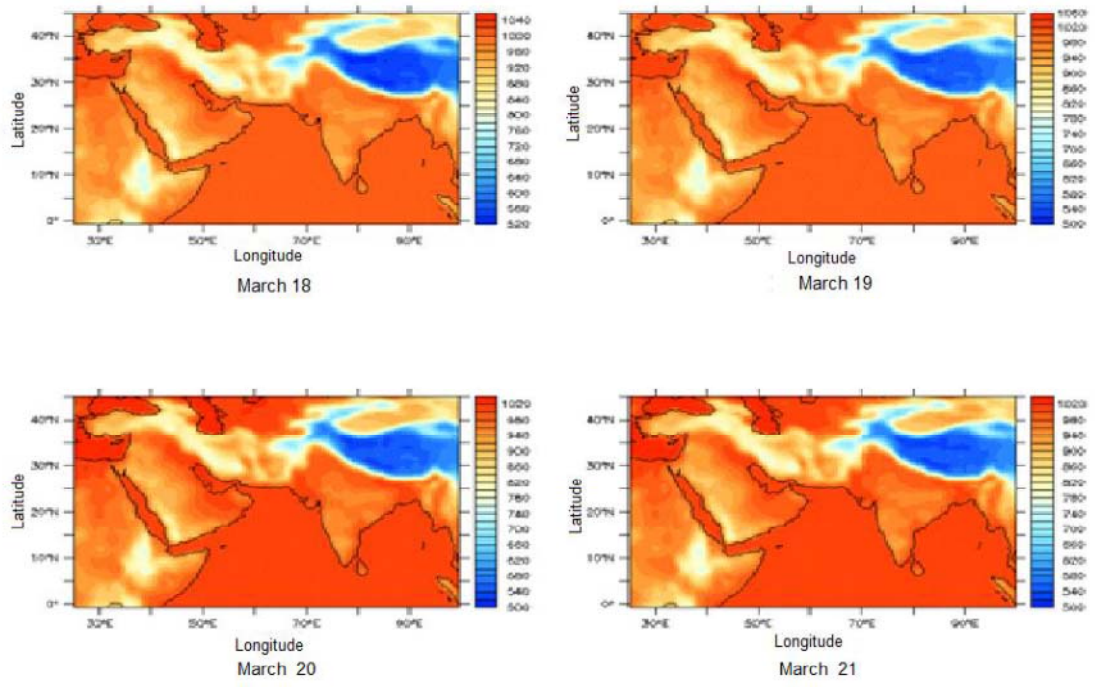


Figure 9

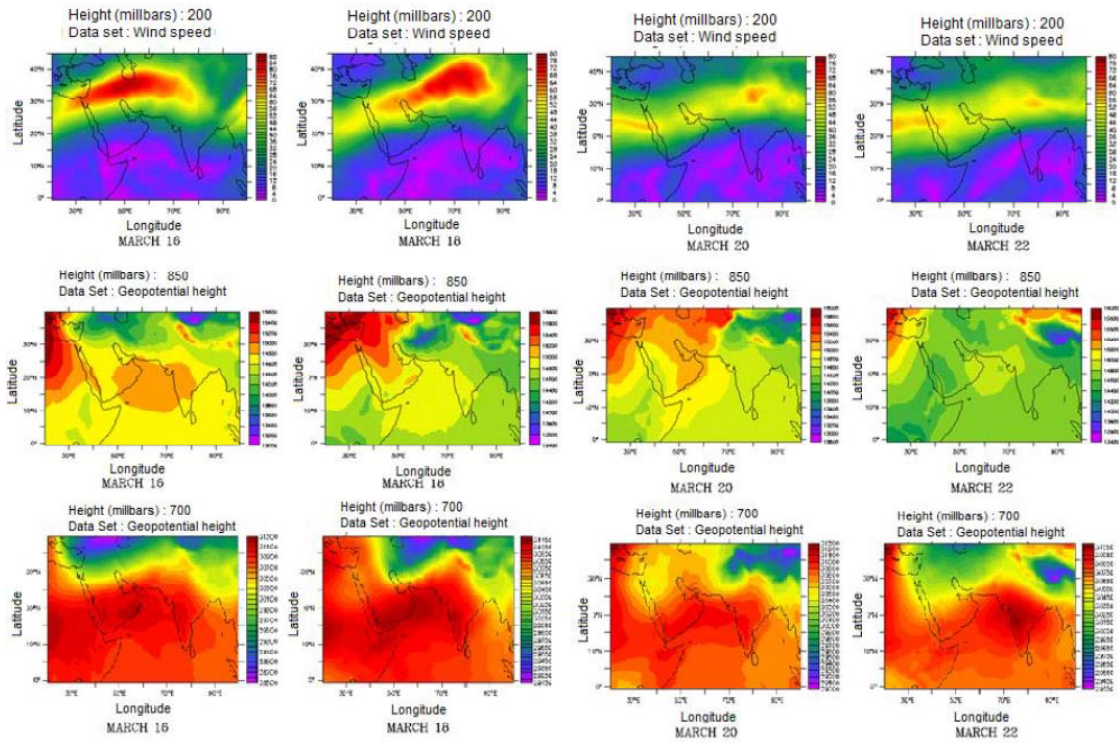


Figure 10

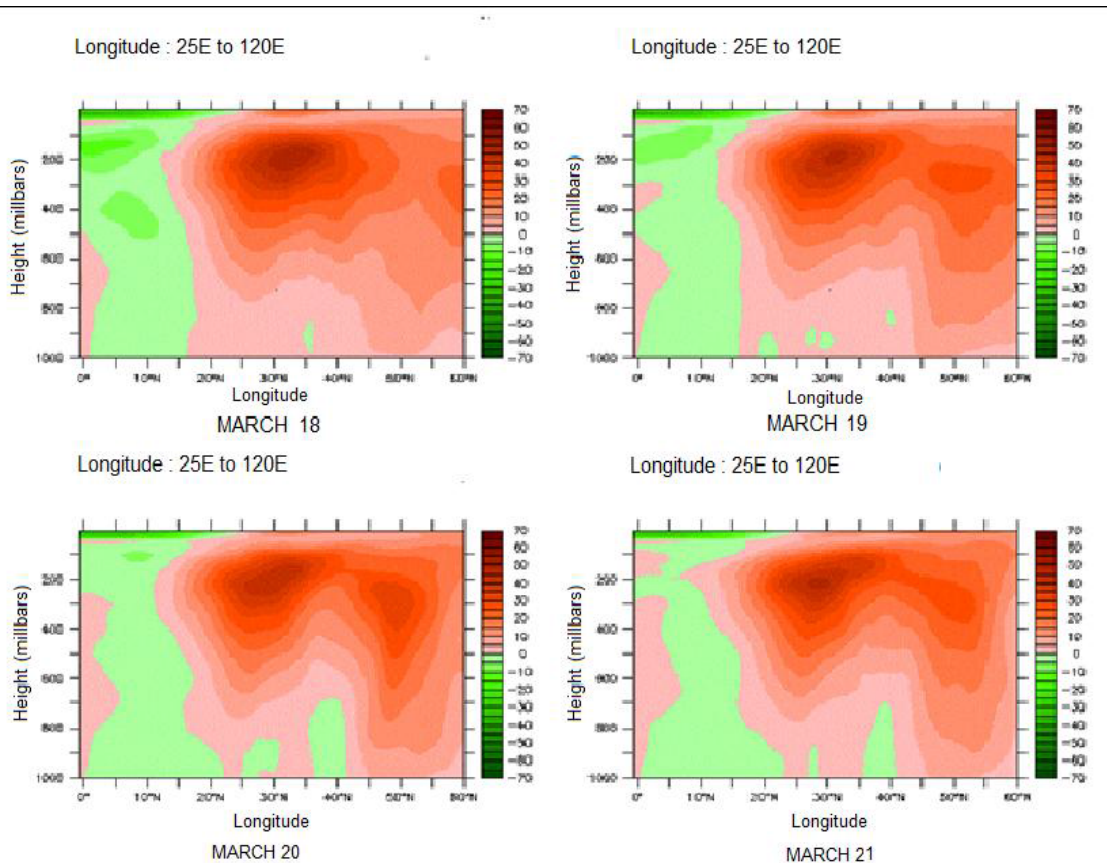


Figure 11

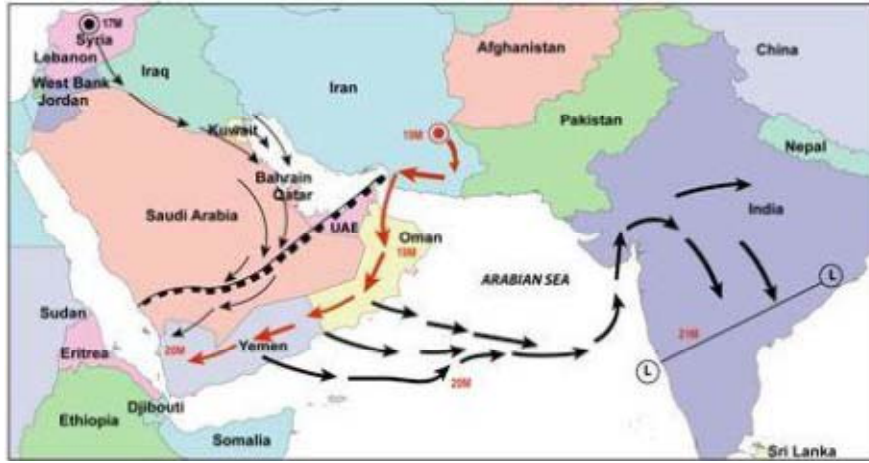


Figure 12

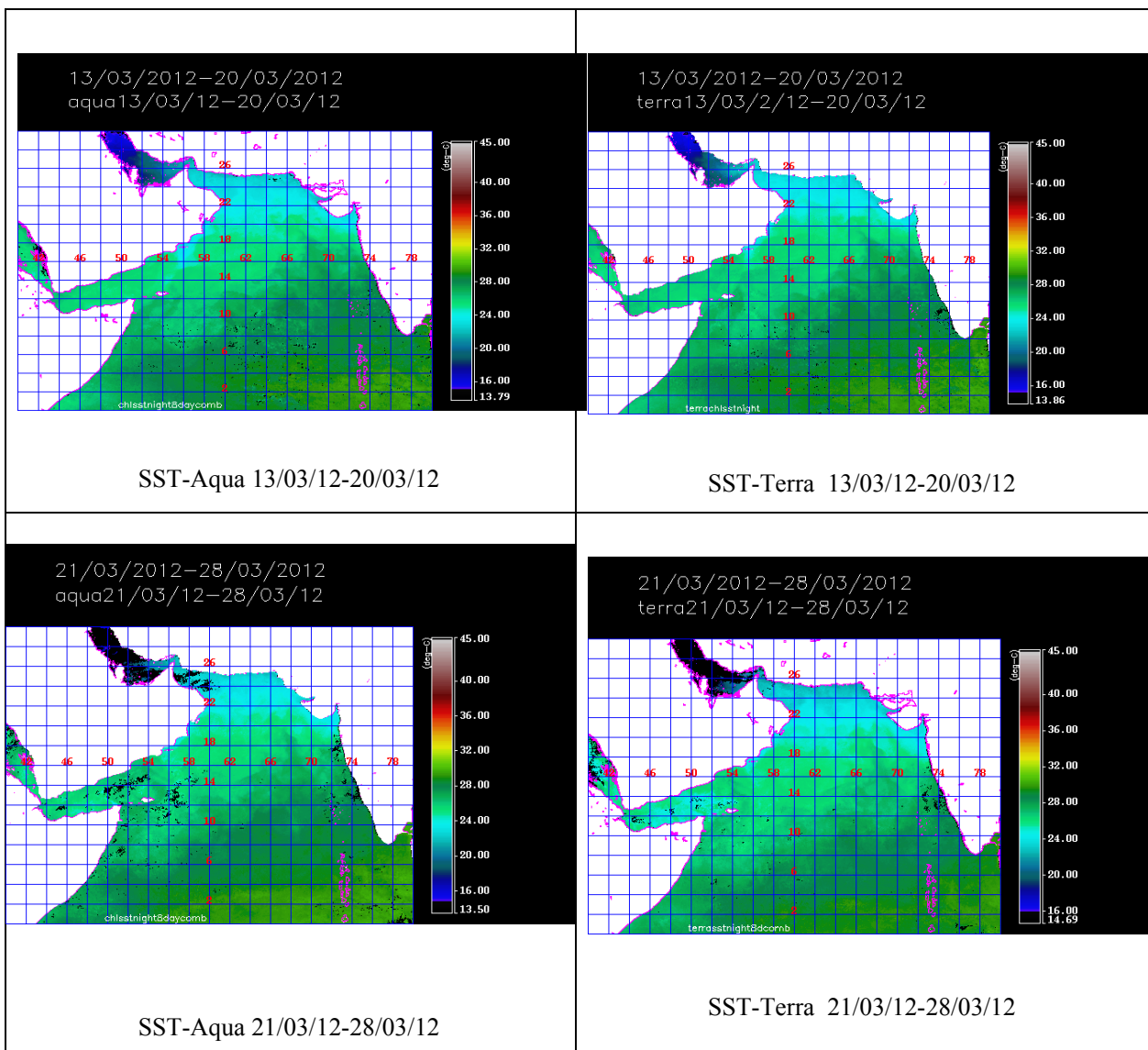


Figure 13

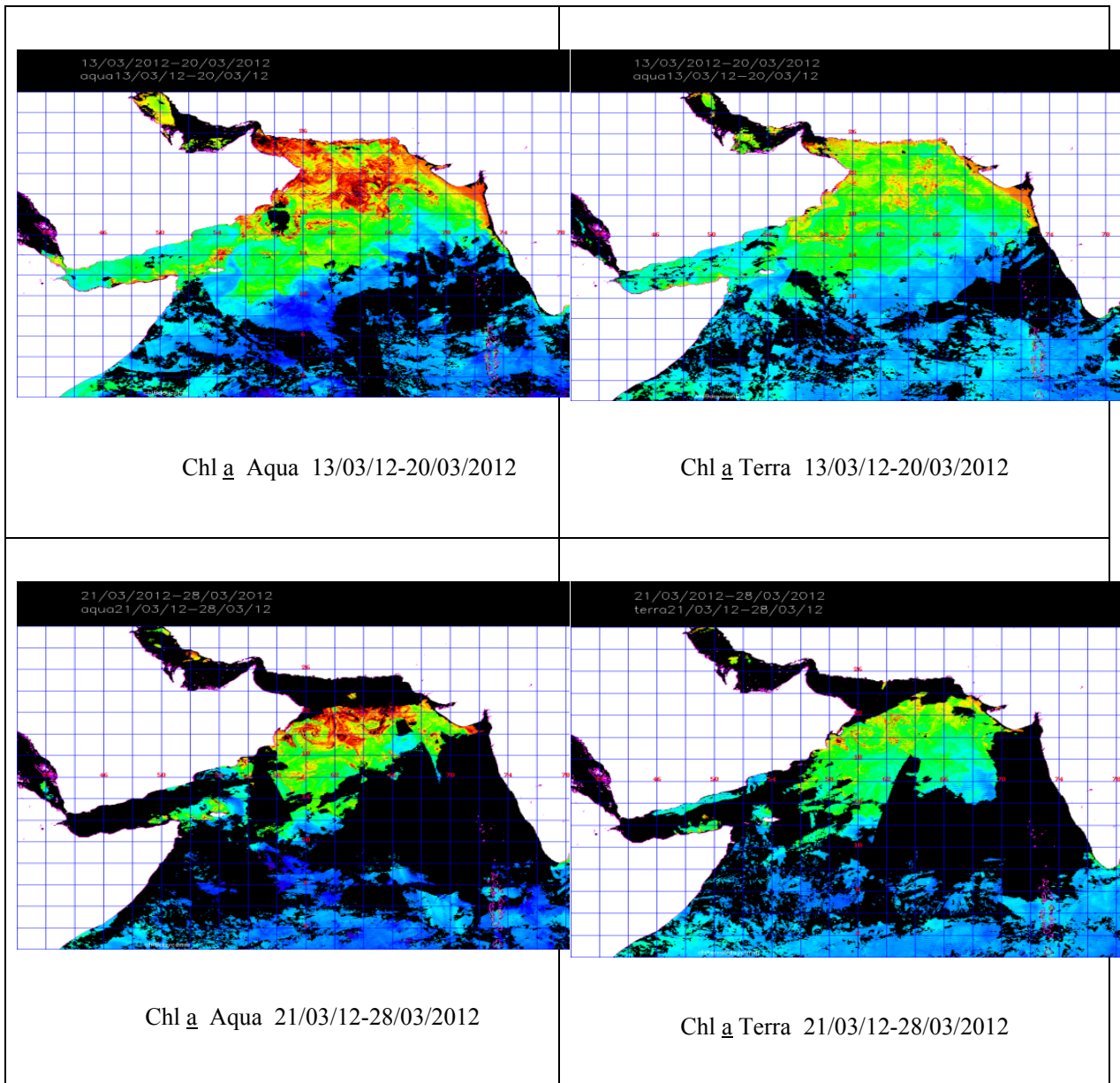


Figure 14

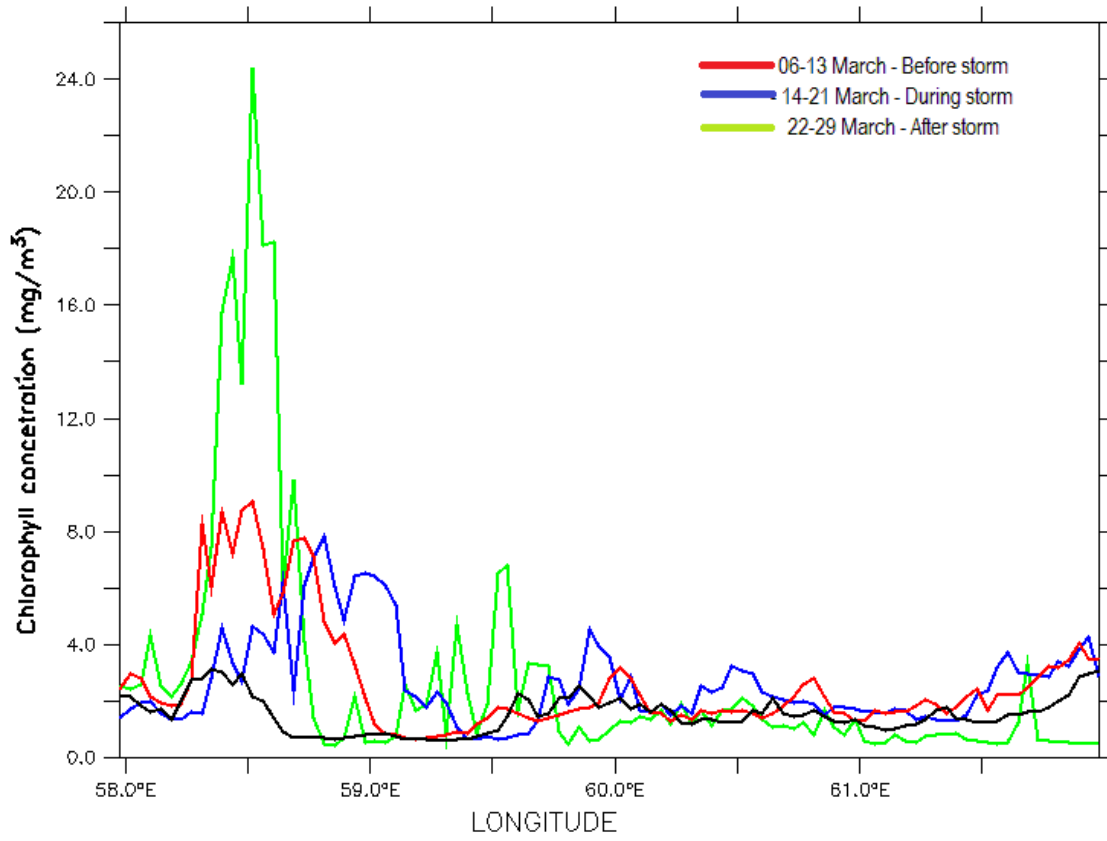


Figure 15



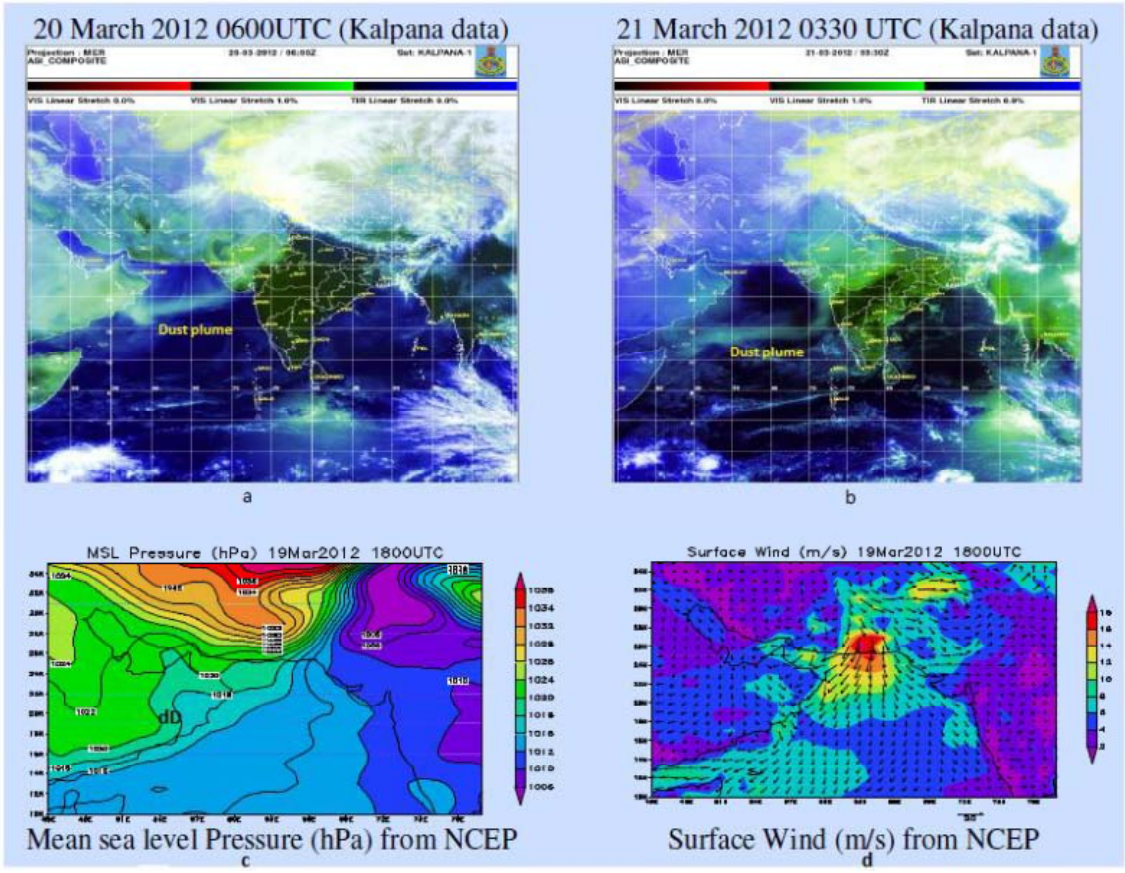


Figure 16